J. Fluid Mech. (2007), *vol.* 589, *pp.* 147–156.
doi:10.1017/S002211200700777X Printed in the United Kingdom

Large-scale features in turbulent pipe and channel flows

J. P. MONTY, J. A. STEWART, R. C. WILLIAMS AND M. S. CHONG

Department of Mechanical Engineering, The University of Melbourne, Victoria 3010, Australia

(Received 4 March 2007 and in revised form 17 July 2007)

In recent years there has been significant progress made towards understanding the large-scale structure of wall-bounded shear flows. Most of this work has been conducted with turbulent boundary layers, leaving scope for further work in pipes and channels. In this article the structure of fully developed turbulent pipe and channel flow has been studied using custom-made arrays of hot-wire probes. Results reveal long meandering structures of length up to 25 pipe radii or channel half-heights. These appear to be qualitatively similar to those reported in the log region of a turbulent boundary layer. However, for the channel case, large-scale coherence persists further from the wall than in boundary layers. This is expected since these large-scale features are a property of the logarithmic region of the mean velocity profile in boundary layers and it is well-known that the mean velocity in a channel remains very close to the log law much further from the wall. Further comparison of the three turbulent flows shows that the characteristic structure width in the logarithmic region of a boundary layer is at least 1.6 times smaller than that in a pipe or channel.

1. Introduction

The last century of wall-turbulence research has seen a strong focus on two areas: statistical analysis and small-scale features very near the wall. Mean velocity scaling and the validity of Kolmogorov's $-5/3$ law are examples. There are numerous reasons to justify this focus, such as the similarity of near-wall behaviour in pipes, channels and boundary layers and the existence of theoretical predictions for flow statistics in the near-wall region. Recently, however, there has been increasing interest in large-scale features, particularly in the boundary layer (e.g. Adrian, Meinhart & Tomkins 2000; Ganapathisubrimani, Longmire & Marusic 2003; Del Álamo *et al.* 2004). These investigations have been successful in explaining previously well-known though unexplained phenomena, such as the high length-to-width ratios observed in two-point correlation maps (Kovasznay, Kibens & Blackwelder 1970) and the highly energetic low-wavenumber modes in the outer region (Guala, Hommema & Adrian 2006). These phenomena may be explained by very long trains or 'packets' of hairpin eddies as proposed by Kim & Adrian (1999, hereafter referred to as KA99). While the packet theory provides a mechanistic framework, further details of the large-scale features throughout the flow are still required, particularly in turbulent pipe and channel flows.

Recently, Hutchins & Marusic (2007, hereafter referred to as HM07) discovered very long meandering features in the logarithmic region of turbulent boundary layers which they term 'superstructures'. These were observed from hot-wire measured

velocity fields in the (x, z)-plane (note that x, y, z represent the streamwise, wall-normal and spanwise coordinates respectively). HM07 report observations of super-structures having streamwise lengths of $O(20\delta)$. Throughout this article, δ refers to boundary layer thickness, pipe radius or channel half-height. Such structures have been documented from particle image velocimetry (PIV) measurements by Ganapathisubramani *et al.* (2003) and Tomkins & Adrian (2003); however in both of these cases the field of view was too small to capture the entire length of the structures. These studies have all shown that the important dimensions of the large structures scale with the boundary layer thickness and therefore do not change with Reynolds number (Re). HM07 go on to say that these structures are not only highly energetic but have a footprint at the wall which makes a significant contribution to the turbulent kinetic energy very near the wall, even down to $y \approx 15\nu/U_\tau$ (where ν is the kinematic viscosity and U_τ is the friction velocity). This is consistent with the attached-eddy hypothesis of Townsend (1976).

It is the principal aim of this investigation to capture the behaviour of the large-scale motions in turbulent pipe and channel flows, employing similar techniques to those used by HM07 in their zero-pressure-gradient boundary layer study.

2. Experimental apparatus

The pipe and channel flow facilities both use air as the working fluid and have roughly the same maximum bulk velocity ($U_{b(max)} \approx 30\,\mathrm{m\,s^{-1}}$) and similar relevant dimensions: the channel half-height, $h = 50\,\mathrm{mm}$, and the pipe radius, $R = 49.4\,\mathrm{mm}$. The hot-wire filaments were platinum of 5 μm diameter and a length-to-diameter ratio of 180–200.

2.1. *Pipe flow*

The pipe flow apparatus was identical to that used by Perry, Henbest & Chong (1986). A feature of this facility is its length ($\sim 400D$); however, the most downstream station was unavailable due to concurrent experiments for another study, so measurements were made at $x = 175D$ (where D is the pipe diameter). Preliminary results from a recent flow development study indicate fully developed flow well upstream of $175D$.

Ideally one would construct an azimuthal hot-wire probe array capable of contracting/expanding to any desired radius of curvature. Unfortunately, it was not possible to construct such an array without causing unacceptable blockage in the confined space of a $\sim 100\,\mathrm{mm}$ diameter pipe. Therefore, two fixed-radius rings were carefully made to house 15 custom-made hot-wire probes. Both rings had the same radius of curvature: the first had an arclength of $1.37R$, while the second had an arclength of $2.34R$. The radius of curvature of the ring centrelines was $R_{hw} = 42\,\mathrm{mm}$ so that each hot wire was nominally located $0.15R$ from the wall (the edge of the commonly defined log region). The longer arc ring is shown schematically in figure 1(*a*). For this ring, the probe spacing was uniformly $0.167R$. With the smaller ring, the central 11 wires were equally spaced $0.08R$ apart, with the remaining wires at $0.13R$ spacing.

At the fixed wall-normal position of $y = 0.15R$, hot-wire voltages were recorded at 9 kHz sampling frequency for 120 s (9 kHz was the maximum possible with simultaneous sampling using a *Microstar Labs 4000a* data acquisition board). These measurements were performed for a range of Reynolds numbers; all relevant parameters are documented in table 1. Over the Re range, 120 s of data corresponds to $\sim 7300\delta/U_{CL} - 73000\delta/U_{CL}$, where U_{CL} is the centreline velocity.

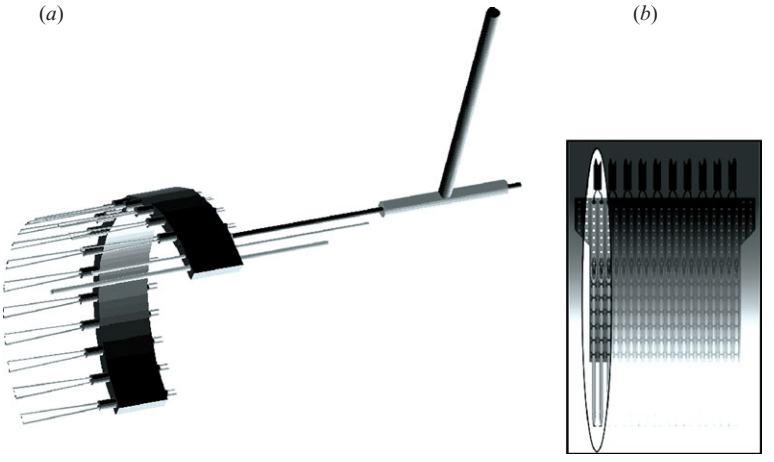

FIGURE 1. Schematic views of (*a*) the semicircular hot-wire rake for the pipe flow measurements and (*b*) the plane array for the channel flow. The light grey tubes mounted at the end of the pipe flow ring are Pitot tubes. One probe of the channel hot-wire array is highlighted with the rest shaded out for clarity.

Arclength $2.34R$				Arclength $1.37R$			
$U_{(y=0.15R)}$	U_τ	Re_τ	Re_b	$U_{(y=0.15R)}$	U_τ	Re_τ	Re_b
26.1	1.26	4212	188924	27.1	1.30	4355	196119
24.1	1.17	3923	174545	24.4	1.19	3966	176686
21.0	1.04	3472	152259	21.1	1.04	3486	152963
17.6	0.89	2968	127758	19.6	0.98	3266	142181
14.2	0.73	2456	103272	18.1	0.91	3043	131350
10.7	0.57	1914	78026	14.6	0.75	2517	106173
7.37	0.41	1384	54106	11.6	0.61	2055	84527
3.91	0.24	793	28715	9.5	0.52	1724	69323
3.34	0.21	686	24328	7.2	0.40	1352	52664
2.88	0.18	615	21432	4.7	0.28	933	34553

TABLE 1. Experimental parameters for the two pipe hot-wire rakes having different arclengths. $Re_b = 2RU_b/\nu$, where U_b is the bulk velocity, and $Re_\tau = RU_\tau/\nu$ is the Kármán number. All velocities have units of $\mathrm{m\,s^{-1}}$.

2.2. *Channel flow*

The channel facility at Melbourne was built only recently and full details are available in Monty (2005). Measurements were taken at $x = 205 \times 2h$ from the sandpaper trip, using a novel spanwise array of 10 hot-wire probes. The array was made from sewing needles and common electronic stripboard. A needle was attached to each of 20 copper tracks on the stripboard by weaving copper wire around the needle and through the holes in the board. Wollaston wire was then soldered to each pair of needles to create 10 hot-wire probes. Figure 1(*b*) illustrates the details of the hot-wire rake. Stripboard has a standard hole spacing of 2.5 mm resulting in probe centres spaced uniformly 5 mm ($0.1h$) apart. Therefore, the total spanwise extent of the array was $0.9h$. With only 10 hot wires a higher sampling rate was possible, so velocity traces of 120 s duration were recorded at 20 kHz sampling frequency. Only one Reynolds number

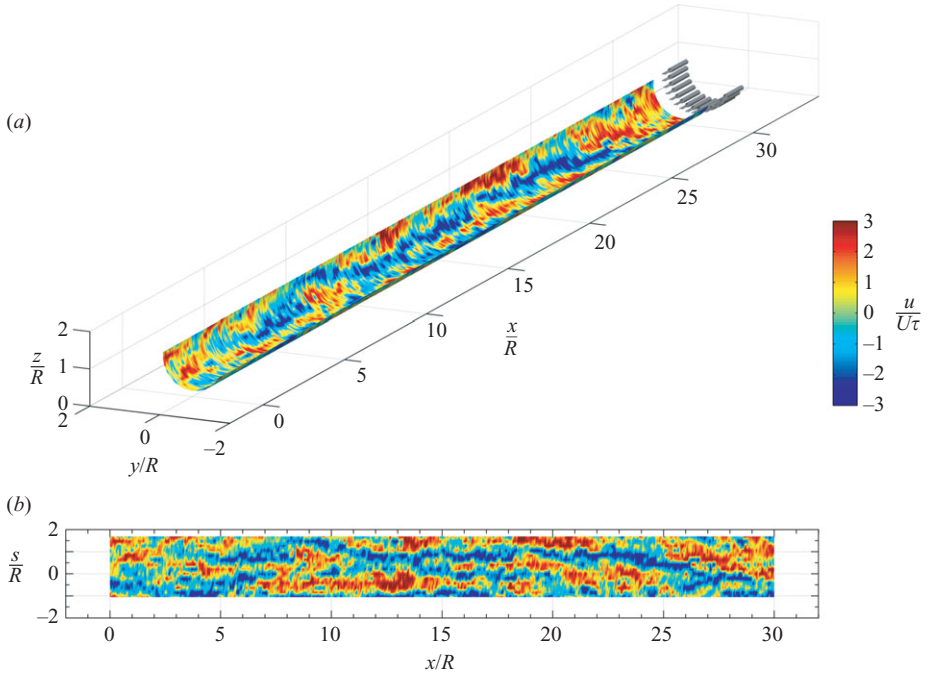

FIGURE 2. Contour plots of streamwise velocity fluctuations measured in the pipe at $Re_\tau = 3472$. The streamwise velocity has been scaled with the friction velocity, U_τ. (*a*) The velocity field in the true coordinate system; (*b*) a transformed view of the field in Cartesian coordinates.

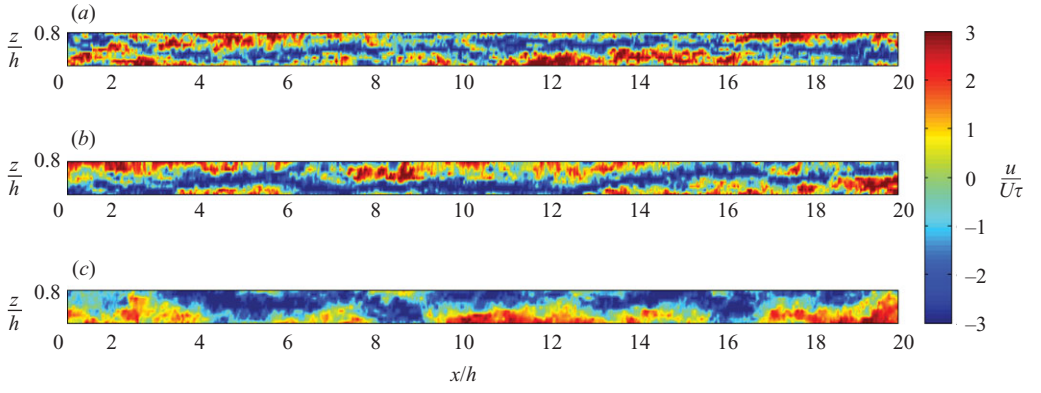

FIGURE 3. Contour plots of streamwise velocity fluctuations measured in the channel with $Re_\tau = 3178$: (*a*) $y = 0.08h$, (*b*) $y = 0.14h$, (*c*) $y = 0.56h$.

was studied, $Re_b = 144\,362$ ($Re_\tau = 3178$), while the wall-normal position was varied from $y = 0.08h$ to $1.0h$. Note that 120 s of data equates to $51960\delta/U_{CL}$ at this Re.

3. Instantaneous velocity fields

Figures 2 and 3 present contour plots of streamwise velocity fluctuations for pipe and channel flows. In arriving at these results, a constant convection velocity equal to the local mean (measured over 120 s) was subtracted from each velocity record to

reveal the field of velocity fluctuations shown. Taylor's frozen turbulence hypothesis has been employed to infer the spatial velocity field from the temporal. Very recent studies in this area by Ganapathisubramani, Clemens & Dolling (2007) and Dennis & Nickels (2007) suggest that Taylor's hypothesis should not significantly alter the large-scale features of figures 2 and 3. In both pipe and channel flows the elongated blue strips meandering over the plane are obvious (the velocity fields shown are typical of those observed throughout the entire data set). The blue low-speed regions flanked by red high-speed regions are the signature of the 'superstructures' from HM07. Thus, it is evident that pipes, channels and boundary layers have a qualitatively similar structure in the log region, even in the largest scales. As with boundary layers, the largest scales seen in the visualization are typically $O(20\delta)$ in length. We had presupposed that much longer structures would be found in the pipes and channels after the work of KA99 and Tsubokura (2005). Tsubokura also showed snapshots from high-Re simulations of pipe and channel flows which are similar to figures 2 and 3. KA99 showed that the large-scale peak in premultiplied streamwise velocity spectra for pipe flow was at a significantly longer wavelength (up to 14δ) than for boundary layers (typically $\sim 6\delta$ according to HM07). It is therefore suggested that the longer energetic wavelengths (lower energetic wavenumbers) in pipe and channel flows most likely result from a greater population of the 5δ–20δ-long features, rather than an increase in the length of the longest features.

Two pipe flow velocity fields are shown in figure 2: one plotted on the true cylindrical plane, the other 'unwrapped' onto a two-dimensional plane. For the two-dimensional plot, the 'spanwise' dimension is $s = \theta R_{hw}$, where θ is the azimuthal position, so that s represents a relative arclength which is then scaled with the radius, R. This choice of coordinate and its scaling may not seem ideal, but it must be remembered that the radius of a circular array diminishes as one moves away from the pipe wall. Thus a coordinate that reflects this behaviour must be chosen in order to compare visualizations (like those in figure 2b) at various wall distances. Figure 2(b) shows that the large structures clearly meander around the plane as reported by HM07 for boundary layers. Interestingly, when viewed in the physically correct coordinate system of figure 2(a), meandering means that structures are precessing around the pipe. If one imagines the blue strips as the fluid encapsulated by a train of attached eddies (see figure 7 of KA99), those eddies are moving from a horizontal orientation to a vertical – a rotation about the axis of symmetry of 90°. In examples not shown here for brevity, structures moving across the entire array were observed, representing rotations about the pipe axis of 180°.

For channel flow, figure 3 displays visualizations at three different distances from the wall. Again there is a meandering of large structures through the field. There are two important observations to be made as the array is lifted from the wall: first, the very long large-scale structures persist at least until $y/h = 0.56$†; second, the width of the structures is visibly increasing with distance from the wall. The former point is unique to pipe and channel flow as there appears to be a breakdown of the large scales outside the log-layer in boundary layers (Ganapathisubramani *et al.* 2003). The increasing width of the structures has also been noted by Hutchins, Hambleton & Marusic (2005) and Tomkins & Adrian (2003) for a boundary layer, although

† The spanwise extent of the hot-wire array ($0.9h$) was insufficient beyond $y/h \approx 0.6$ due to the increasing spanwise length scales. Plots beyond this point revealed only wide high- or low-speed patches, so no information concerning streamwise length was inferable.

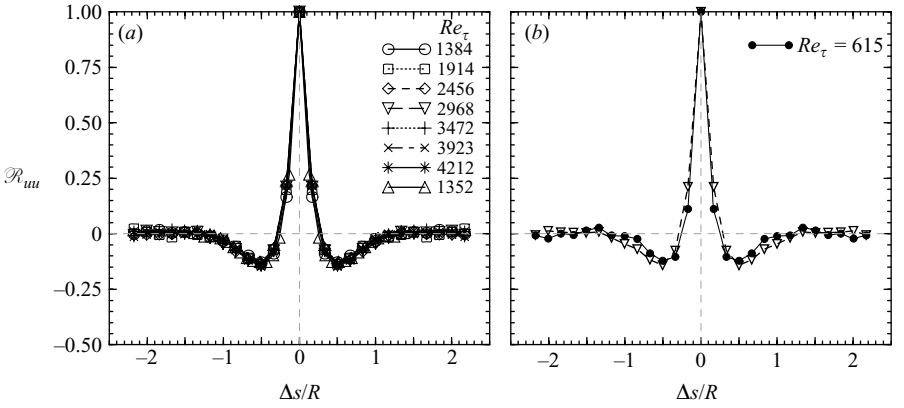

FIGURE 4. Pipe flow two-point correlations at $y = 0.15R$. (*a*) $Re_\tau > 1000$. Note the last data set, △, was taken with the smaller hot-wire array and so has improved small-scale resolution. (*b*) Lowest-Reynolds-number data, $Re_\tau = 615$, with $Re_\tau = 2968$ for comparison.

it is much more prevalent in the channel. Further investigation into the large-scale structure width is the subject of the following section.

4. Streamwise velocity correlations

So far only qualitative conclusions can be drawn from the images presented. Statistical analyses are now required to establish average structure characteristics. For this purpose, the two-point streamwise velocity correlation coefficient across the spanwise array,

$$\mathscr{R}_{uu}(\Delta s, y) = \frac{\langle u(s,t)u(s+\Delta s,t)\rangle}{\langle u(s,t)^2\rangle}, \tag{4.1}$$

is employed. Here, s is a coordinate along the array (z for the channel), u is the fluctuating component of streamwise velocity and angle brackets indicate a spatial and temporal average. Beginning with pipe flow, the correlations are plotted in figure 4. The first interesting aspect of this figure is the strong negative–positive–negative correlation trend, which is indicative of hairpins or counter-rotating streamwise vortex pairs, in an average sense. Furthermore, there is complete collapse of the correlations across all $Re_\tau > 1000$. This supports the boundary layer findings of HM07 who showed outer scaling of the correlation over a three orders-of-magnitude Reynolds number range. Interestingly, the spanwise extent of positive correlation is approximately $0.58R$ which gives a measure of the characteristic width of the eddies at the edge of the log region. Note that this is significantly wider than that typically reported in boundary layers (according to HM07); § 4.1 discusses this point in more detail. In figure 4(*b*), the lowest-Reynolds-number two-point correlations are shown along with higher-Re data for comparison. At first glance the plots appear to collapse reasonably well, indicating that the large structures scaling with outer variables are still prevalent at low Re_τ. However, a closer inspection reveals slightly lower correlation at small Δs as well as oscillations in the $Re_\tau = 615$ correlations. The latter phenomenon is also seen in the DNS (direct numerical simulation) data of Moin & Spalart (1987) and is most likely due to lack of convergence. The former difference can be described by an insufficient range of scales at such a low Re_τ. If we consider the height of the smallest eddies (Kline scales) to be $h_K^+ = O(100)$ following Perry & Chong (1982),

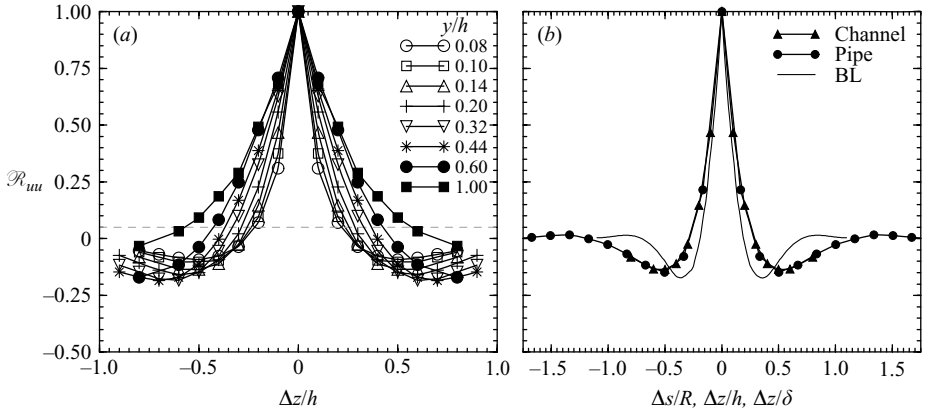

FIGURE 5. (*a*) Two-point correlations for channel flow at $Re_\tau = 3178$ with varying wall distance. (*b*) Comparison of the two-point correlation curve for moderate-to-high Reynolds number pipe, channel and boundary layer flows at $y = 0.15\delta$. The boundary layer (BL) data come from HM07.

then Kline streaks are intersecting the hot-wire array which is at $y^+ = 0.15Re_\tau = 92$ for this Reynolds number (the superscript '+' denotes scaling with the viscous length scale, ν/U_τ). These small-scale streaks will tend to 'pinch' the correlation, leading to reduced correlation at low values of Δs and may even influence the noted oscillatory behaviour at larger Δs (if Kline streaks and superstructures interact as proposed by HM07).

Turning to the channel flow data shown in figure 5(*a*), where wall-normal location was varied at a fixed Re_τ, the increasing width of the structures observed in the velocity fields of figure 3 is now clearly shown to be characteristic of the shear flow. Furthermore, the increasing width with wall distance is consistent with Townsend's (1976) attached-eddy hypothesis. It is also interesting that the negative–postive–negative correlation behaviour, characteristic of coherent structures, persists throughout the flow, as might be expected in a shear flow that is entirely turbulent (there is no 'free stream' in a channel).

Finally, figure 5(*b*) compares typical two-point correlations for mid-to-high Re boundary layer, pipe and channel flows at $y = 0.15\delta$. It is immediately obvious that the boundary layer correlation differs greatly from the pipe and channel flows; the pipe and channel results are almost identical. Although the qualitative behaviour of all the correlations is similar, the difference lies in the scaling of the abscissa. Simply increasing the length scaling in the pipe/channel flow cases from δ to 1.64δ results in good collapse of all correlations at this wall distance. This is a somewhat surprising result given that all wall-bounded turbulent shear flows have long been considered similar up to the edge of the log region. Before drawing any conclusions about this observation, a quantitative analysis of the spanwise width scale in pipes, channels and boundary layers is required.

4.1. *Spanwise width scale growth*

A better understanding of the growth of coherent structures with wall distance can be gained from plotting the quantity l_z, defined as the difference between the Δz (or Δs for pipe flow) values at which the correlation value is $R_{uu}(\Delta z) = 0.05$ (this correlation threshold is marked on figure 5*a* with a dashed line). Thus l_z represents the average width of all turbulent structures at a given distance from the wall. In figure 6(*a*), this

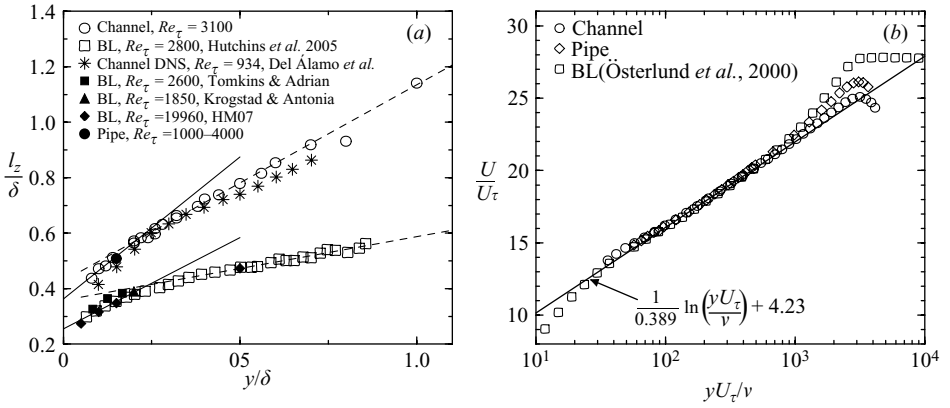

FIGURE 6. (*a*) Variation of spanwise width scale, l_z, with wall distance. Solid lines are curve-fitted to open symbols for $y > 0.15\delta$; dashed lines are fitted to open symbols where $y > 0.4\delta$. The slopes of the lines are 1.022 (solid), 0.707 (dashed) and 0.657 (solid), 0.229 (dashed) for the channel and boundary layer respectively. (*b*) Comparison of mean velocity profiles in pipe, channel and boundary layer flows with $Re_\tau \approx 3200$. The pipe and channel data come from Monty (2005).

width scale is plotted for the channel flow data (○) and compared with boundary layer data (□) from Hutchins *et al.* (2005). Also included are boundary layer data available in the literature as well as channel flow DNS data from Del Álamo *et al.* (2004).

The most striking aspect of this figure is the difference between the channel/pipe and boundary layer width scales. Although these very different flows were not expected to behave similarly far from the wall, the differences observed extend well into the log region. Inside this region (say, $y < 0.15\delta$), it could be argued that l_z increases linearly for both channel and boundary layers, although at different rates (linearity in various measures of spanwise scales in the log region has been shown by Tomkins & Adrian 2003 and Hoyas & Jiménez 2006). However, beyond the log region, the channel structures quickly assume a new constant growth rate, which continues to the centreline. It has been claimed that the logarithmic region is longer in channels (Zanoun, Durst & Nagib 2003), yet this abrupt structural change evidenced by the l_z behaviour is in support of the traditional log region limits. The boundary layer behaves quite differently, with l_z more slowly peeling off toward a lower growth rate which is also constant. This difference in growth rates (slopes of l_z) indicates that outer-flow channel structures grow approximately three times faster than those in a boundary layer.

It is conjectured that this behaviour may be explained by the persistence of the coherence of structures beyond the log region in a duct. Outside the log region of a boundary layer, coherent structures (e.g. KA99's hairpin packets) that exist in the log region do not retain their coherence as they grow to heights exceeding 0.15δ (Marusic 2001). The breakdown of these structures produces a population of smaller eddies which may be detached eddies, vortex rings or some other outer-layer structure (Perry & Marusic 1995). In regard to the two-point correlation, the effect of smaller scales on the field of the remaining largest scale structures will be to 'pinch' the positive section of the correlation curve, as described earlier, thereby reducing the spanwise width scale, l_z. However, for channel flow, coherent structures stubbornly persist well beyond the log region, which suggests a smaller population of

broken-down small scales ('small' refers not to eddies scaling with viscous units, but to large eddies that are not as large as they might be if they remained coherent during their growth from the wall). Further evidence for this persistent coherence is provided by comparing mean velocity profiles as shown in figure 6(*b*). Clearly the pipe and channel mean velocity profiles lie closer to the log law than boundary layer flows beyond $y = 0.15\delta$. Since very long coherent structures are now known to populate the log region of boundary layers (see HM07 or Ganapathisubramani *et al.* 2003), it is logical to suggest that a more logarithmic mean velocity implies extended streamwise coherence of structures further from the wall. This 'persistent coherence' may also explain the aforementioned lower-wavenumber peak in duct flow energy spectra compared to boundary layers: more coherent structures growing out from the log region are available to form the very long hairpin packets (termed 'VLSM's by KA99) which are assumed to cause that energetic peak.

Also in figure 6(*a*), an l_z value has been included for the pipe flow case. Since the pipe hot-wire array permitted measurements at only one wall distance, only one data point was obtainable; nevertheless, correspondence with the channel data is remarkable. Clearly then, a difference in spanwise length scales for pipe/channel and boundary layer flows has been confirmed. This is an indication that the traditional largest length scale for pipe or channel flow (h or R) should be reconsidered, although no definitive argument can be made based on two-point correlations alone. Also requiring further investigation is the scaling of l_z for pipe flow as wall distance increases. In figure 6(*a*) the pipe radius has been used for this scale; however, pipe data cannot continue to follow the channel beyond the log region as the limits of the coordinate $s = \theta R_{hw}$ diminish with distance from the wall (because R_{hw} is decreasing). A study of pipe flow spanwise length scales in the outer region would therefore be interesting from a conceptual point of view.

5. Conclusions

Novel arrays of hot wires have been used to experimentally analyse the spatial behaviour of turbulent pipe and channel flows. Using Taylor's frozen turbulence hypothesis, two-dimensional velocity fields have been plotted, revealing long meandering features throughout the flow. These features appear qualitatively similar to those reported for boundary layers and have similar lengths of $O(20\delta)$.

The spanwise two-point correlation of streamwise velocity appears to be identical at the edge of the log region in pipes and channels, and both display qualitative behaviour similar to published boundary layer data. From the correlation plots, it was found that the width of the characteristic large-scale structures increases with distance from the wall. This was expected and is consistent with Townsend's attached-eddy hypothesis. Interestingly, the structure width markedly changes behaviour beyond the traditional inner region limit in both channels and boundary layers, suggesting traditional log-law limits are applicable to channel flow. In the log region, large structures were found to be approximately 1.6 times wider in the pipe or channel than in the boundary layer. It is therefore tentatively suggested that an increase in the outer length scale usually employed for pipes and channels by a factor of $\sim$1.6 may be appropriate. Finally, the largest-scale structures grow at a greater rate with distance from the wall in a channel. This provides further evidence of persisting coherence of eddies and packets of eddies beyond the log region of a pipe/channel flow and is in contrast to boundary layers where such structures are reported to break down at comparable distances from the wall.

The authors are grateful for the financial support of the Australian Research Council through the Discovery Projects scheme (DP0556629).

REFERENCES

Adrian, R. J., Meinhart, C. D. & Tomkins, C. D. 2000 Vortex organization in the outer region of the turbulent boundary layer. *J. Fluid Mech.* **422**, 1–54.

Del Álamo, J. C., Jiménez, J., Zandonade, P. & Moser, R. D. 2004 Scaling of the energy spectra of turbulent channels. *J. Fluid Mech.* **500**, 135–144.

Dennis, D. & Nickels, T. B. 2007 Something about validation of taylor's hypothesis in a turbulent boundary layer. In *Proc. 11th European Turbulence Conference, Porto, Portugal*.

Ganapathisubramani, B., Clemens, N. T. & Dolling, D. S. 2007 Effects of upstream boundary layer on the unsteadiness of shock induced separation. *J. Fluid Mech.* **585**, 369–394.

Ganapathisubramani, B., Longmire, E. K. & Marusic, I. 2003 Characteristics of vortex packets in turbulent boundary layers. *J. Fluid Mech.* **478**, 35–46.

Guala, M., Hommema, S. E. & Adrian, R. J. 2006 Large-scale and very-large-scale motions in turbulent pipe flow. *J. Fluid Mech.* **554**, 521–542.

Hoyas, S. & Jiménez, J. 2006 Scaling of the velocity fluctuations in turbulent channels up to $Re_\tau = 2003$. *Phys. Fluids* **18**, 011702.

Hutchins, N., Hambleton, W. T. & Marusic, I. 2005 Inclined cross-stream stero particle image velocimetry measurements in turbulent boundary layers. *J. Fluid Mech.* **541**, 21–54.

Hutchins, N. & Marusic, I. 2007 Evidence of very long meandering features in the logarithmic region of turbulent boundary layers. *J. Fluid Mech.* **579**, 1–28.

Kim, K. C. & Adrian, R. J. 1999 Very large-scale motion in the outer layer. *Phys. Fluids* **11**, 417–422.

Kovasznay, L. S. G., Kibens, V. & Blackwelder, R. F. 1970 Large-scale motion in the intermittent region of a turbulent boundary layer. *J. Fluid Mech.* **41**, 283–325.

Krogstad, P. A. & Antonia, R. A. 1994 Structure of turbulent boundary layers on smooth and rough walls. *J. Fluid Mech.* **277**, 1–21.

Marusic, I. 2001 On the role of large-scale structures in wall turbulence. *Phys. Fluids* **13**, 735–743.

Moin, P. & Spalart, P. R. 1987 Contributions of numerical simulation data bases to the physics, modeling and measurement of turbulence. *Tech. Rep.* 100022. NASA.

Monty, J. P. 2005 Developments in smooth wall turbulent duct flows. PhD thesis, The University of Melbourne.

Österlund, J. M., Johansson, A. V., Nagib, H. M. & Hites, M. H. 2000 A note on the overlap region in turbulent boundary layers. *Phys. Fluids* **12**, 1–4.

Perry, A. E. & Chong, M. S. 1982 On the mechanism of wall turbulence. *J. Fluid Mech.* **119**, 173–217.

Perry, A. E., Henbest, S. & Chong, M. S. 1986 A theoretical and experimental study of wall turbulence. *J. Fluid Mech.* **165**, 163–199.

Perry, A. E. & Marusic, I. 1995 A wall-wake model for the turbulence structure of boundary layers. Part 1. Extension of the attached eddy hypothesis. *J. Fluid Mech.* **298**, 361–388.

Tomkins, C. D. & Adrian, R. J. 2003 Spanwise structure and scale growth in turbulent boundary layers. *J. Fluid Mech.* **490**, 37–74.

Townsend, A. A. 1976 *The Structure of Turbulent Shear Flow*, 2nd edn. Cambridge University Press.

Tsubokura, M. 2005 LES study on the large-scale motions of wall turbulence and their structural difference between plane channel and pipe flows. In *Proc. Fourth Intl Symposium on Turbulence and Shear Flow Phenomena, Willamsburg, VA*.

Zanoun, E.-S., Durst, F. & Nagib, H. 2003 Evaluating the law of the wall in two-dimensional fully developed turbulent channel flows. *Phys. Fluids* **15**, 3079–3089.